OPEN ACCESS

Saudi Journal of Civil Engineering
Abbreviated Key Title: Saudi J Civ Eng
ISSN 2523-2657 (Print) | ISSN 2523-2231 (Online)
Scholars Middle East Publishers, Dubai, United Arab Emirates
Journal homepage: https://saudijournals.com/journal/sjce/home

Original Research Article

Geotechnical, Mineralogical, Petrographic and Microstructural Characterization of Two Lateritic Gravels from Congo

Sorel Dzaba Dzoualou[2], Louis Ahouet[1,2,3]*, Sylvain Ndinga Okina[1,2], Prince Nkembo Mang[2], Paul Louzolo-Kimbémbé[2]

[1]Higher Institute of Architecture, Urbanism, Building and Public Works, Denis Sassou Nguesso University, Congo
[2]Higher National Polytechnic School (ENSP), Marien Ngouabi University – Brazzaville, Congo
[3]Control office for Building and Public Works (BCBTP) – Brazzaville, BP 752, Congo

DOI: https://doi.org/10.36348/sjce.2024.v08i09.002 | **Received:** 04.10.2024 | **Accepted:** 14.11.2024 | **Published:** 16.11.2024

***Corresponding author:** Louis Ahouet
Higher Institute of Architecture, Urbanism, Building and Public Works, Denis Sassou Nguesso University, Congo

Abstract

The recovery of lateritic gravel contributes to the reduction of road construction costs and environmental impact. These materials are of particular interest in road construction because of their abundance, especially in tropical countries, as in the case of Congo. The results obtained on the soils of ‘‘TSANGA and TSIAKI’’ show an identical appearance of the two particle size curves, with more fines in the TSANGA sample. Both soils are moderately plastic and their properties predispose them to mechanical treatment (TSIAKI soils) and hydraulic binders (TSANGA soils). The lateritic gravels of TSIAKI can be used as road sub-base for medium traffic while those of TSANGA as sub-base for low traffic. The geotechnical properties of the two samples differ due to the mineralogy, petrography and microstructure which vary from one deposit to another. The SEM microstructure study shows two matrices completely made of kaolinite and the matrix facies are cemented by hematite. X-ray microscopy and SEM allowed the differentiation of goethite and hematite to distinguish the two forms of iron oxides. The TSIAKI soil has a normal iron oxide content (mainly goethite), and has less quartz and kaolinite, which could justify its high CBR index.

Keywords: Lateritic gravels, Mineralogy, Petrography, Road geotechnics, Microstructure.

1. INTRODUCTION

Road infrastructure is one of the essential elements for the socio-economic development of a country. In developing countries, road infrastructure is essentially dominated by dirt roads. For example, in the Republic of Congo, unpaved roads represent 20.123 km or 86.61% of the road network [1]. Dirt roads are often covered with lateritic gravel, with a life span of one to two years. Under the combined actions of traffic, rainfall and inadequate maintenance, these roads degrade by losing all or part of their wearing course [2]. Indeed, some studies have shown that lateritic gravels, although not meeting the specifications of European or American standards, have proven to be good in road construction, whereas some roads built in compliance with these same standards have deteriorated prematurely [2-5]. This can be explained by the fact that these standards were designed with the behavior of materials in temperate climates in mind. However, road construction and maintenance in developing countries is hampered by high construction costs and environmental impact [4, 6]. The use of appropriate local materials seems to be the ideal solution to reduce such costs [5-8]. Furthermore, the use of non-conventional local materials (recycled, treated or natural) can be an asset if preceded by the necessary geotechnical studies [6-10]. Indeed, lateritic gravels are among the most used local materials in road construction, especially in tropical countries due to their abundance [11, 12]. This soil is sensitive to water, loses the fine fraction due to wind and runoff, and to road undulations generated by vehicle traffic. This is the case of G3 lateritic gravels, which have an unstable behavior after their compaction in the pavement body [13]. The use of lateritic gravel in the construction of earth roads requires special arrangements. Although very varied, studies on lateritic gravel have not exhausted the subject. Therefore, many studies for the use of these materials in road construction only focus on classical geotechnical characterization, which often does not provide sufficient information on the behavior of lateritic soils [14]. For each lateritic gravel deposit, it is important to carry out the necessary tests; for example, by associating

mineralogical analyses, etc. with the classic geotechnical tests, as suggested by certain authors [14, 15]. Consequently, the aim of this work is to characterize the lateritic gravels of the Congo by combining classical geotechnical tests with mineralogical, petrographic and microstructural analyses. Indeed, the behavior of lateritic gravels depends not only on the granularity but also on the mineralogy, microstructure and petrography. The results of this study will contribute not only to the evaluation of the properties of use of these materials in road construction, but also to the quantification of the variability of the geotechnical properties of TSANGA and TSIAKI lateritic gravels, in relation to their microstructure and the environment.

2. MATERIAL AND METHOD

2.1 Material

The geological map [16], at 1:200,000 indicates a basement of Neo-Proterozoic age, constituted by the Lower Diamictite and Sandstone group, which includes the Lower Diamictite, Louila-Bouenza and Upper Diamictite formations. The Lower Diamictite is characterized by a shaly and sometimes sandstone matrix, generally massive, containing pebbles and blocks of 3 cm to 3 m, quartzite sandstone, quartzite, quartz-feldspathic base, rhyolite and black or blue cherts. Intercalations of quartzites and shales appear locally. Based on the information obtained from the geological documents, a survey of the outcrops in the study areas and a detailed analysis were carried out in situ. Two lateritic gravel samples were collected in the south of the Republic of Congo in the Niari and Bouenza departments according to the respective geographical coordinates; TSANGA (S 0410'19.5"; E 012 52'17.4") and TSIAKI (S 04 10'34.1"; E 013 28'40.4"). Approximately 250 kg of material was taken from each site for laboratory testing.

2.2 Method

In the laboratory, the samples were subjected to geotechnical tests and microstructural and petrographic analyses.

Tests of Geotechnical Properties

Particle Size Analysis

The particle size curve represents the percentage distribution of solid grains according to their size. For particle separation, two types of tests were carried out: by sieving for grains of size ϕ>80 µm according to the NF P94-056 standard [17], and by sedimentation for grains of diameter $\phi \leq 80$µm in accordance with the NF P94-057 standard [18]. The uniformity coefficients Cu and curvature coefficients Cc were used to characterize the grain size of the soils, according to the following formulae:

$C_U = \frac{D_{60}}{D_{10}}$ (1)

$C_C = \frac{D_{30}}{D_{60}}$ (2)

D_x - is the grain size corresponding to x % by weight of sieve.

Atterberg Limits

The Atterberg limits were determined according to the Casagrande method (NF P 94-051) [19]. The plasticity index, liquidity and plasticity limits are the three parameters that determine the plasticity of a soil. In practice, they indicate the sensitivity of a soil to changes in its water content. The liquid limit (LL) separates the liquid state from the plastic state; the plastic limit (PL) separates the plastic state from the solid state; the plasticity index measures the extent of the soil's plasticity domain. The plasticity index PI characterizes the extent of the water content range in which soils exhibit plastic behavior.

LL and PL are determined on the fraction of soil (mortar) passing the 0.40 mm aperture sieve. The plasticity index is expressed by the following relationship:

$PI = L_L - L_P$ (3)

The modulus of plasticity of the material is obtained by multiplying the 425 mm passes by the plasticity index PI (%).

Soils Classification

Depending on the physical and chemical properties of the grains, the soil is classified by one or more classification systems: (1) classification for gravelly soils, where more than 50% of the elements by weight are above 80 µm and (2) classification for fine soils, where more than 50% of the elements by weight are below 80 µm. The classification of the Road Earthworks Guide GTR92 (standard NF P 11 300) [20] is used to distinguish the two lateritic gravels.

Methylene Blue Value (MBV)

The methylene blue value (MBV) is determined from the methylene blue spot test on a 0/2 mm fraction. The value found is related to the 0/50 mm fraction by a rule of proportionality. This test is used to characterize the clay content (or cleanliness) of a soil. It represents the quantity of methylene blue that can be adsorbed on the external and internal surfaces of the clay particles contained in the soil fraction analyzed. It is a quantity directly linked to the specific surface of the soil and which globally reflects the quantity and quality (activity) of its clay fraction. The blue value of the soil is determined from the methylene blue spot test on a 0/2 mm fraction, according to the standard N FP 94-068 [21].

Modified Proctor (Maximum Dry Density)

The Modified Proctor Test is used to determine the optimum moisture content (OMC) for which compaction leads to a maximum dry weight. The maximum dry density (MDD) is not a direct indication of the mechanical strength of the soil. However, for a material that nevertheless has pores, the more interactions there are between the particles, the better the cohesion of the soil. The water content of the soil can be influenced by the mineralogy and the formation environment which influence the water content of the

soil. The optimum moisture content (OMC) and maximum dry density MDD were measured using the modified Proctor test in accordance with NF P94-093 [22].

The CBR Test

California Bearing Ratio allows us to perform mechanical characterization of natural and compacted soils in embankments and subgrades, road and airport foundations and sub-foundations. It measures the shear strength of a soil and the swelling of the soil when immersed in water for 4 days. It allows us to calculate the bearing capacity of soil, estimating its resistance to punching. This test is used all over the world to determine the thickness of foundation layers, establish a classification of soils and allow the study of traficability. It can be performed in-situ and in the laboratory, but the latter option is not often carried out. It gives us indispensable parameters in geotechnical testing prior to construction. There are different types of CBR tests to be performed depending on the type and quality of the soil. The standard that definishes this test is NF P 94-078 [23].

Los Angeles Test

The Los Angeles test measures the combined resistance to impact and progressive deterioration by mutual friction of the elements of an aggregate. This procedure applies to aggregates used in the construction of pavements and hydraulic concrete. The European standard EN 1097-2 [24] describes the Los Angeles test.

Microstructure, Mineralogy and Petrography Analyses

The microstructure of the samples was determined by polarizing optical microscopy and scanning electron microscopy. Scanning electron microscopy (SEM) coupled with EDS gives information on the relief of the sample, the morphology of the grains and their arrangement in the material. After SEM analysis, the samples were tested with the energy selection spectrometer using two different methods:

a) Acquisition of X-EDS point and/or average spectra over a small window of the sample area scanned by the primary electron beam in phase contrast (backscattered electrons). Each spectrum allows the identification of all chemical elements in the area scanned by the primary beam. Quantification using the ZAF matrix correction gives the concentration (At %) of each of these elements. As the EDS spectra are acquired in a primary vacuum, on a sample with low conductivity, the quantification obtained (also done without reference standards) is semi-quantitative. The mineralogical interpretation of the quantifications (At %) obtained in this way allows the mineralogy of the samples to be characterized.
b) 2D EDS X-ray mapping acquisitions. This acquisition mode allows to obtain 2D elemental maps of all the chemical elements identified on an average EDS spectrum over the area to be mapped. Each mapping allows the identification of areas rich and poor in a particular element. In this acquisition mode, an X-EDS spectrum is acquired in each pixel of the 2D area scanned, which can be subsequently processed by a statistical approach (phase reconstruction) to produce a 2D map of the phases (minerals) making up the area analyzed.

The X-ray diffraction analyses (XRD) to take stock of the qualitative balance of the different crystallized mineral species present are carried out on a SIEMENS D500 Diffractometer. This apparatus is equipped with a BRAGG BRENTANO geometry goniometer of the diffractometry center and is used for all X-ray characterizations. The fine fraction of the samples (% pass < 80µm) is used to perform the XRD.

The Riedvelt method was applied to quantify and determine the different mineral phases. Indeed, after detection of the mineral phases, they were quantified by the Riedvelt method. This method consists of simulating a diffractogram from the ICDD database and gradually adjusting the closest diffractogram model; the chemical composition corresponding to the closest simulation of the diffractogram model is thus considered as the chemical composition of the sample. For petrography, all slides were observed using a Leica DM750 P optical microscope with a polarizer and analyzer.

DTA/GTA analyses coupled with mass spectrometry were used to determine the main thermal accidents in the samples.

3. RESULTS

3.1 Geotechnical properties of TSANGA and TSIAKI lateritic gravels.

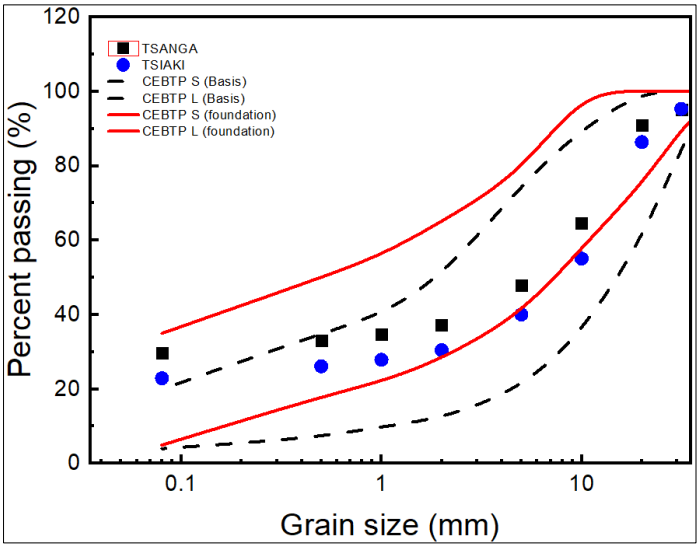

Fig. 1: Grading curves (TSIAKI, TSANGA) and normative curves for lateritic gravels that can be used in sub-base and base courses of paved roads.

The results obtained from curve 1 (Fig.1) are contained in Table 1.

Table 1: Particle size characteristics of TSANGA and TSIAKI lateritic gravels

Soil	D_{max} mm	P (%) 80μm	P (%) 2mm	P (%) 40mm	Cc	Cu
TSANGA	31.5	29.68	37.52	100	1.25	-
TSIAKI	40	22.91	25	100	8.27	-

D_{max}- maximum grain diameter, P - sieve passing's, Cc - coefficient of curvature, Cu - coefficient of uniformity.

From Fig.1, the TSANGA grading curve fully integrates the normative sub-base curve. For the normative spacing of the base course of a road, the grains of size 0.5 mm are at the upper limit of the spacing and at 0.08 mm, the curve passes above the normative spacing (percentage of fines of 29.68% is higher than the maximum of 20%) [25]. The TSIAKI lateritic gravels fit well into the normative spindle from the base layer up to grain size 0.2 mm. Beyond that, the curve goes above the normative range (the percentage of fines of 22.91% is higher than the maximum of 20%) [25]. For the normative spindle of the sub-base layer, the grain sizes between 5 mm and 10 mm are below the lower normative limit (the particle size curve goes out of the spindle). For grains of 2 mm, the curve is at the lower normative limit of the sub-base course spindle. In order for the two lateritic gravels to integrate the two normative spindles, they should be improved with a soil less rich in fines, and the percentage of grains between 2 mm and 10 mm should be increased for the TSIAKI sample. Moreover, the two particle size curves have a similar appearance to those observed for other lateritic gravels. Indeed, without being identical, these curves generally fit within the spindle for the coarse elements and are flared for the fine elements [3]. The maximum grain diameter of the TSANGA and TSIAKI sample is 31.5 mm and 40 mm respectively, above the lower size of 10 mm and below the maximum size of 50 mm [25, 26]. The passing's at 80 µm are 29.68% and 22.91%, below the upper limit of 35% for the sub-base materials, but above the upper limit of 20% for the base materials [25, 26]. The curves are not uniform because the uniformity coefficient is not measurable (i.e., both curves have passing's above 10%). The grain distribution in the TSANGA soil is well calibrated Cc (1.25), (i.e., $1 < Cc < 3$) and poorly calibrated for the TSIAKI Cc (8.27). Table 2 gives a summary of the geotechnical characteristics of the soils studied.

Table 2: Geotechnical characteristics of TSANGA and TSIAKI lateritic gravels

Soil	DDMT/m^3	OMC (%)	FB (%)	FA (%)	CBR (%)	LA	PM	LS (%)	LL (%)	PL (%)	PI (%)	SBV (%)
TSANGA	1.95	10.63	30	35	27	35	436	0.7	26	12.8	13.2	2.2
TSIAKI	2.198	7.43	23	27	68	30	421	0.4	27	10.2	16.2	4.3

DDM - maximum dry density, OMC - optimum moisture content, FB - percentage of fines before compaction (passes over 80µm), FA - percentage of fines after compaction, CBR - bearing index, LA - Los Angeles, MP - plasticity modulus, LS- linear swelling, LL – liquidity limit, PL - plasticity limit, PI - plasticity index, SBV – soil blue value.

The PI of TSANGA and TSIAKI vary respectively from PI (13.2-16.2%), but below the recommended maximum of 30%. Both lateritic gravels are moderately plastic and suitable for use in pavement sub-base. The linear swelling measured in the CBR LS test (0.4-0.7) was below the maximum of 1% for lateritic gravels in pavement base courses [25, 26]. However, the maximum dry density of the TSANGA and TSIAKI samples varies from DDM (1.95-2.198 t/m^3) respectively. The dry density of TSIAKI is higher than the recommended minimum of 2.0 t/m3 for use as a base course and that of TSANGA is between 1.8-2.0T/m3 for use as a pavement base course. The CBR bearing capacity (at 95% of OPM after immersion) of TSIAKI is 68%, higher than the minimum 30% required for sub-base, but lower than the 80% required for pavement base [25, 26]. This bearing capacity is higher than that of lateritic gravels studied in the Democratic Republic of Congo, Ivory Coast and Niger [27-28]. The TSIAKI lateritic gravelly material has a passage at 40 mm of 100%, at 2 mm of 25% (between 20-50%), at 80 m of 22.91% (between 10-25%), the plasticity index PI (16.2), lower than 20 and a CBR (68%) higher than the maximum of 60% [25].

TSIAKI gravel can be significantly improved for use in pavement base courses, if about 30% by weight of 0/40 angular stony aggregate is added; less than 30% of 2 mm pass and less than 18% of 80 µm pass, with a zero-plasticity index and a CBR at 95% OPM of about 90 [25]. The TSANGA lateritic gravel has a CBR index (27%), lower than the minimum of 30% required for pavement sub-bases [25]. On the other hand, the CBR of TSANGA is lower than that of several lateritic gravels studied in Senegal [29]. Nevertheless, by increasing the thickness of the lateritic gravel with a CBR ≥ 25 can be admitted as a pavement base course for low traffic [25]. However, it would be wise to improve the physical-mechanical properties of TSANGA lateritic gravel with hydraulic binders. Indeed, its plasticity index PI is higher than 10%, the passing at 0.425 mm are 33%, higher than the lower limit of 15%, the passing at 80 µm are lower than 35%; the maximum grain size 10-50mm and its plasticity modulus of 436 is lower than 2500, conditions required for the material to be treated with hydraulic binders [25].

The percentages of fines after compaction are respectively 27-35%, an increase of 4% for the TSIAKI sample and 5% for the TSANGA sample. These increases of 4% and 5% are below the recommended maximum of 8% [25]. The methylene blue values (MBV) of TSIAKI and TSANGA MBV (2.2-4.3), (2.5 < MBV < 6), the soils have medium plasticity. The Los Angeles coefficient of the two lateritic gravels of TSIAKI and TSANGA is respectively LA (30-35%), lower than the maximum of 50% [25]. In relation to the specifications of the Road Earthworks Guide GTR92, the two lateritic gravels are of class B6, like most of the lateritic gravels studied [3-20]. The petrography, mineralogy and microstructure of the two materials are determined below.

Petrography, Mineralogy and Microstructure of the Two Lateritic Gravels

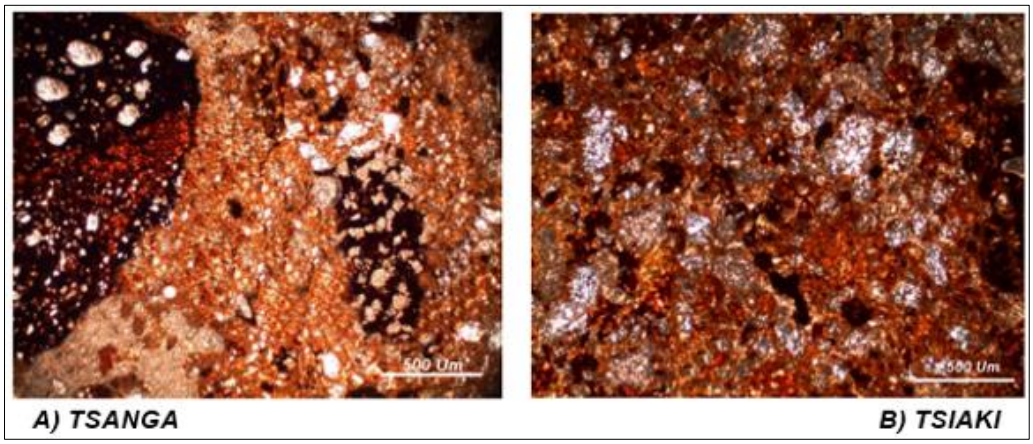

Fig. 2: Polarized natural light observation (LNPA; x4 magnification) of thin sections of the TSANGA and TSIAKI samples. The grey-beige color represents the amorphous resin; the ochre, white, orange and yellow-orange colors represent the various minerals that appear.

From Fig.2, the texture of these samples is represented by isolated accumulations of iron oxides mainly in an aggregate of quartz grains, all wrapped in a kaolin matrix. Quartz particles were detected in the matrix, but at a relatively lower density compared to the cementing zone.

The petrographic study of the samples revealed various minerals such as kaolinite, quartz and iron oxide. According to the combination and distribution of the elements, two types of textures are distinguished:

The texture with detached ferruginous action represented by the TSANGA sample. It has very iron-rich zones with high silica contents. These zones are isolated and unevenly spread in the kaolinic matrix poor in iron oxide. Fissured quartz grains are also interspersed in the kaolinite matrix. The spread iron-action texture represented by the TSIAKI sample. Absorption by iron oxides occurs through the natural porosity of the matrix. The iron oxides attack all the facies present in the matrix through the porosity, fill the voids and create bridges between the textural elements.

The distribution of iron oxides is not privileged. The matrix is completely composed of kaolinite. The diffractograms and Riedvelt quantification of the two lateritic gravels are defined from Figure 3.

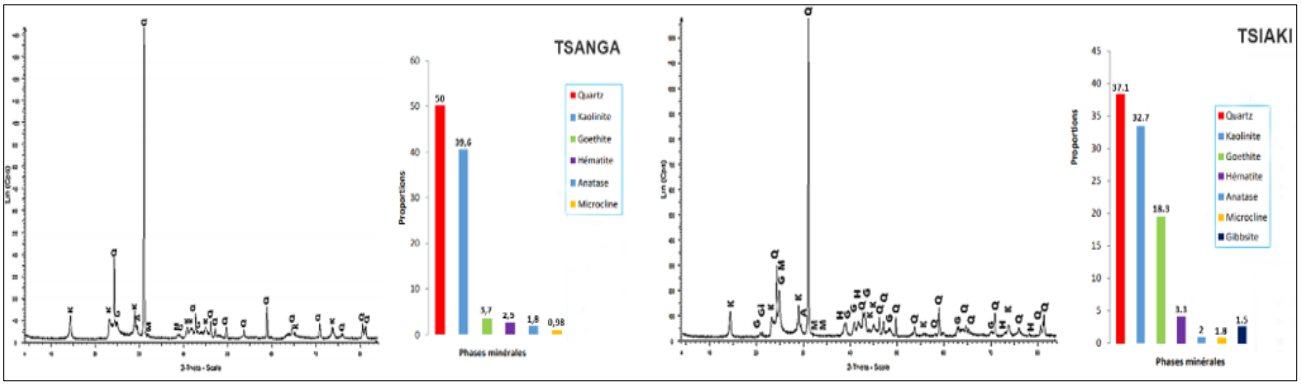

Fig. 3: Diffractogram and Riedvelt quantification of TSANGA and TSIAKI samples

XRD analysis revealed the presence of crystallized minerals in the samples. Kaolinite, goethite, anatase, hematite, microcline and quartz are present. However, the TSANGA sample is the only sample that contains hydrated aluminum oxide (gibbsite Al (OH)3). These minerals are present in the samples analyzed and present very different percentages from one sample to another. The minerals present are:

The TSANGA sample shows some traces of Titanium oxides (anatase) and microcline (1.8 and 0.98). There are also high levels of kaolinite and silica, respectively 39.6 and 50%. The iron oxides (goethite and hematite) present have very low contents of the order of 3.7% and 2.5%.

The TSIAKI sample has quartz as the dominant mineral with a content of 37.1% and kaolinite is 32.7%. The kaolinite and quartz contents are lower than in TSANGA.

However, iron oxides are well represented with high contents of 18.3% for goethite and 3.3% for hematite. Aluminum oxides (gibbsite) were also identified in the TSIAKI sample as well as the presence of anatase and microcline (2% and 1.8%).

From this analysis, quartz and kaolinite are dominant with respective contents between 32.7% - 50% and 32.7% - 39.6%. The low silica content found in the TSIAKI sample can be explained by the low rainfall in the department (dry season) which causes less leaching and less dominant alteration of the geological formations in place. A large quantity of silica could not be released during leaching, resulting in a lower synthesis of kaolinite content. This lesser leaching did not affect the lateritic gravelly horizon, making any induration possible. Furthermore, the TSANGA and TSIAKI samples have iron oxides in proportions of 3.3% and 18.3% respectively. Table 3 shows the XRD data for the two soils.

Table 3: Mineral species content identified by XRD

	Quartz	Kaolinite	Goethite	Hematite	Anatase	Microcline	Gibbsite	TOTAL
TSANGA	50	39,6	3,7	2,5	1,8	0,98	0	98,58
TSIAKI	37,1	32,7	18,3	3,3	2	1,8	1,5	96,7

Figure 4 shows the main thermal accidents determined from DTA/TGA analysis coupled with mass spectrometry.

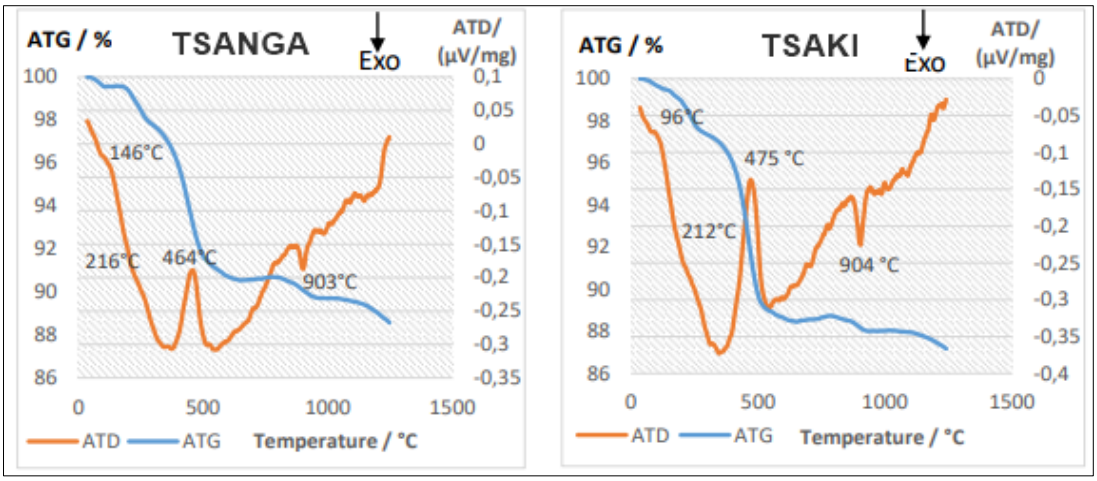

Fig. 4: ATD/ATG curves of TSANGA and TSIAKI laterites

Analysis of the DTA-GTA curves (Fig. 4) identifies four main thermal accidents. The temperature ranges corresponding to these accidents are given in Table 3; the mass losses related to the chemical transformations are presented in Table 4 and 5.

Table 4: Temperatures corresponding to mass departures and gains

Sample	Temperatures representing thermal accidents			
	Water outflow zeolitic	Transformation of Goethite to hematite	Dehydroxylation of kaolinite	Structural reorganisation of meta kaolinite
TSANGA	146	216	464	903
TSIAKI	96	212	475	904

Table 5: Mass losses due to chemical transformations during firing

Sample	Pertes de masses liées aux accidents thermiques				
	Water outflow zeolitic	Transformation of Goethite to hematite	Dehydroxylation of kaolinite	Structural reorganisation of meta kaolinite	Total loss
TSANGA	-0,41	-1,82	-7,15	-2,05	-11,4
TSIAKI	-0,5	-2,19	-8,67	-1,44	-12,8

The XRD and petrographic analyses revealed quartz contents in both samples. These contents were detected by the ATD/ATG analysis, in particular following the manifestation of an endothermic peak between 580 and 620°C during the transformation of quartz from the α form to the β form. After further analysis of the thermograms, the peak relating to this transformation could not be located and the peaks of the transformation of goethite to hematite are not identifiable due to the scale. Figure 5 shows the optical microscope and SEM images of the TSANGA sample.

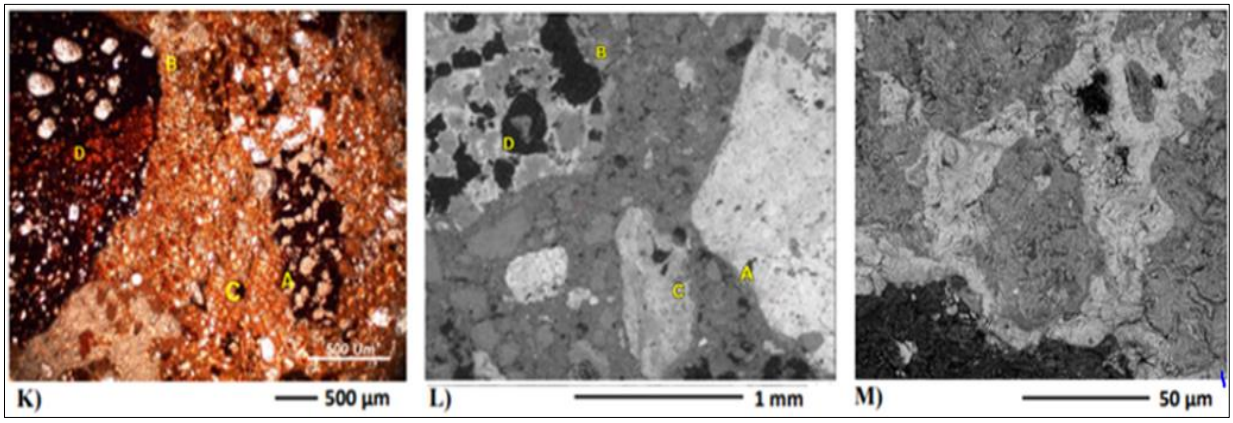

Fig. 5: TSANGA sample. K) Image of the thin slide photographed by optical microscope. L) SEM image of the thin slide. M) Zoom on area C of image L

Figure 5-K is the image taken by light microscopy; then identified by SEM (Figure 5-L) for X-ray microanalysis by EDS. Spectra were collected from four areas. The magnification of zone C (Fig.5-M) shows a combination of a multitude of kaolinite/silica blocks bound by iron oxide cement (hematite). Figure 6 presents details of the chemical elements found in the TSANGA sample.

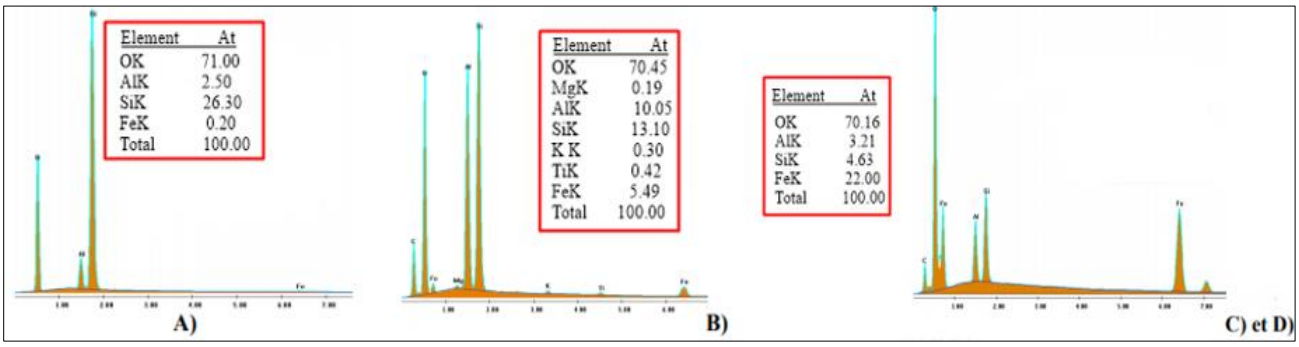

Fig. 6: TSANGA sample. A) Spectrum of zone A with a high concentration of silica B) Spectrum of zone B with a high concentration of kaolinite. C) and D) Spectra of areas C and D with a dominant silica/kaolinite mixture

Zone A (Fig.5-L and Fig.6-A) has a zone of mainly silica and kaolinite with trace Fe oxides. Zone B (Fig. 5-L and Fig. 6-B) has a very high concentration of kaolinite associated with silica and a low content of Fe oxides. Zones C and D (Fig.5-L and Fig. 6-C and D) have the same mineralogical composition and show kaolinite, quartz and a high proportion of iron oxides. Interpretation of the quantification (At%) by the classical correction method (ZAF) does not give the possibility of specifying whether it is goethite or hematite associated with the apparent O content which remains qualitative. Figure 6 shows the Raman spectra collected from zones A, C and D in Figure 5-L. The peaks found in this spectrum are perfectly consistent with the characteristic peaks of hematite in zones C and D and quartz in zone A. Zones C and D therefore consist of more hematite mixed with kaolinite and silica. Figure 7 shows the texture of the TSIAKI sample.

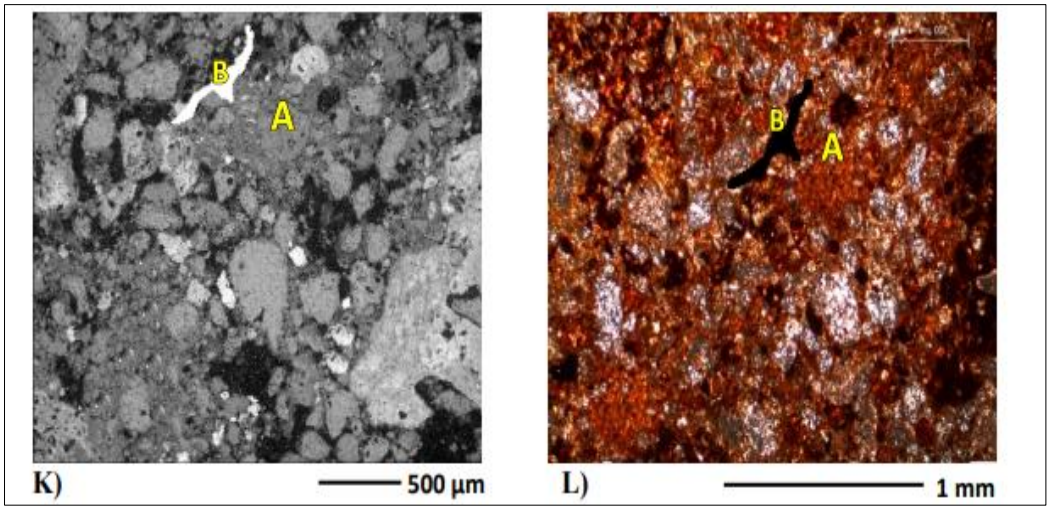

Fig. 7: TSIAKI sample: texture with diffuse iron attack. K) Image of thin slide photographed by optical microscope. L) SEM image of thin slide.

The optical microscope image in Figure 7-K shows that there are no regions of preferential accumulation of iron oxides. They are dispersed throughout the matrix, particularly in the voids. After locating this SEM image (Fig.7-L), two areas were selected for X-ray microanalysis. Zone A (Fig.7-L and Fig.8-A) is represented by a high content of kaolinite (93%) combined with silica (6.3%) and traces of iron oxides whose mineralogical nature is difficult to identify. In Zone B (Fig.7-L and Fig.8-B), the kaolinite content is lower (27.5%), mixed with a significant amount of hematite (64.4%) and 5% silica in Figure 7-L.

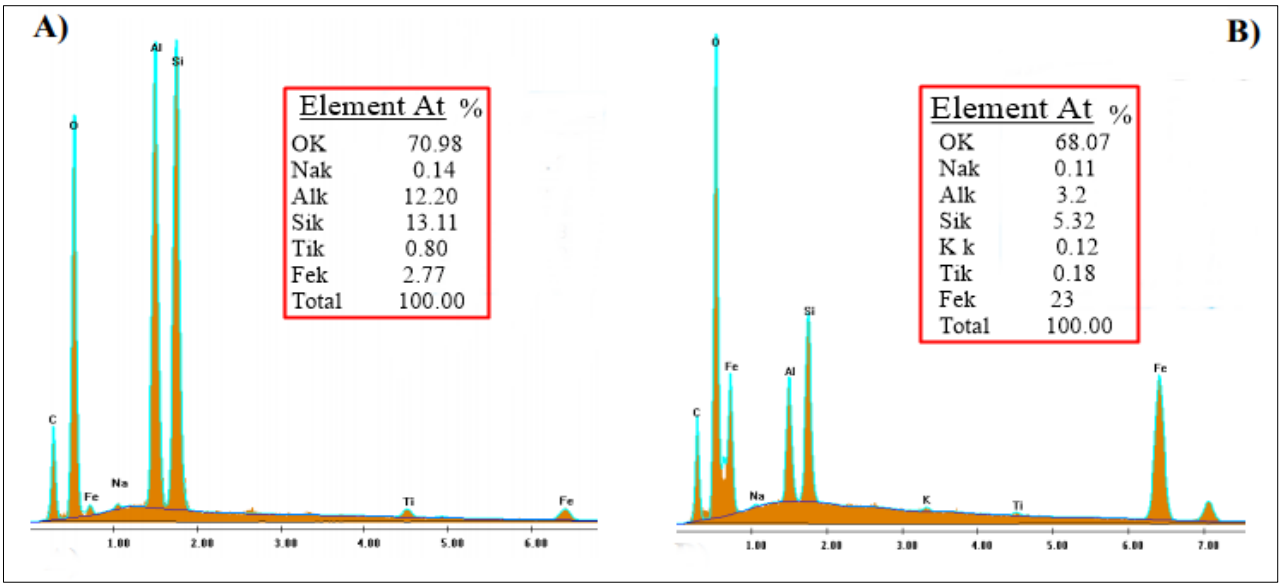

Fig. 8: TSIAKI sample. A) Spectrum of zone A, high concentration containing kaolinite. B) Spectrum of zone B represented by high levels of iron oxides and kaolinite.

Figures 9 and 10 show EDS microanalysis by X-2D mapping of the TSANGA and TSIAKA samples.

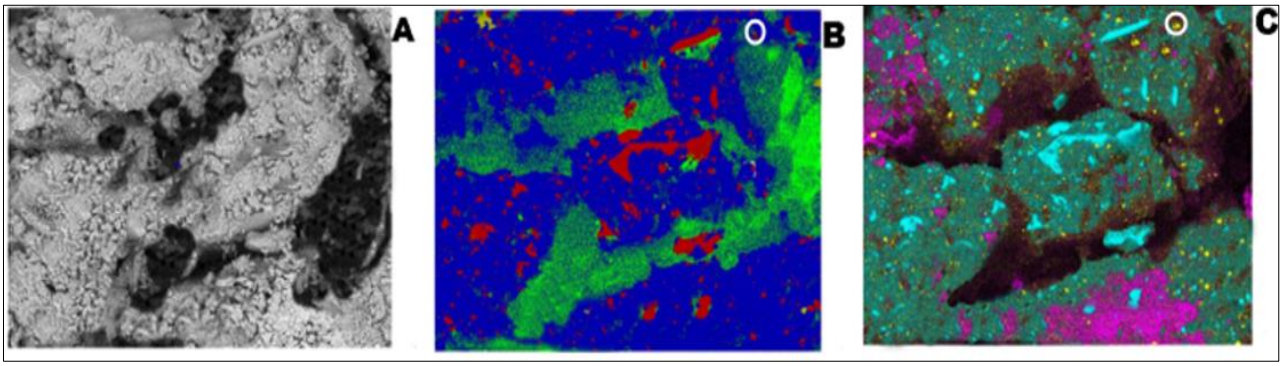

Fig. 9: EDS microanalysis by X-2D mapping of TSANGA samples. Mineralogical composition of TSANGA samples: mapping of mineral phases.

From Figure 9, A) is a BSE (backscattered electron) mode image under low pressure conditions (50 Pa). The bright areas represent heavy atoms (atomic number Z of heavy atomic elements) due to the irregular surface of the sample. B) Mapping resulting from the statistical analysis of the spectral data. The small yellow spots are sections of carbon tape that were used to fix the sample. It is therefore not included in the sample. Areas occupied by the phases: 16% for the red phase, 61% for the blue phase, and 15.5% for the intergranular voids (Green image 9-B).

C) Superposition of the elemental maps, Si in cyan, Fe in violet and Ti in yellow. The black areas are not located by EDS (intergranular porosity, slopes or reliefs not oriented towards the EDS detector and/or constitute areas inaccessible to the incident electron beam), (See green areas in photo 9-B).

The backscattered electron image shown in Figure 9-A taken at the GAD (Gaseous Analytical Detector) has a granular structure with many interstitial cavities. EDS X-ray mapping over the entire area of the Figure 9-B image allowed chemical analysis of the TSANGA sample. After gathering the spectra per image pixel from the facts found; recalculate the (average) spectrum over any part of the mapped area of the small area identified by the white circle in Figure 9-B and C.

Two major phases were identified in the samples (Fig. 9-B and Fig.10). The amount occupied by each of these phases (identified statistically) is shown in Figure 10.

The acquired phase reconstruction is shown in Figure 9-B. In the middle of a phase, the brighter the color of the pixel, the closer the local spectrum of that pixel is to the typical spectrum of the phase displayed statistically.

The phase spectrum characterizing all the red pixels in Figure 9-B in the sense of an average is shown

in Fig.10-A. This spectrum is accompanied by its quantification (At %) by the ZAF method and the mineralogical interpretation that we have made of it. The quantification of the spectrum (Fig.10-A) of the red phase in Figure 9-B is interpreted as a mixture of 60% silica, 33% kaolinite and 7% goethite. The quantification spectrum (Fig.8-B) of the blue phase in Figure 9-B is explained as a mixture of 4% silica, 1.5% anatase (TiO2), 15% goethite and 75% kaolinite.

Superimposing the elemental mappings of Si, Fe and Ti in Figure 9-C shows that the spectrum of Figure 8-B represents the blue phase of Figure 9-B in the sense of an average and that locally the relative abundance of the different minerals composing this blue phase can change.

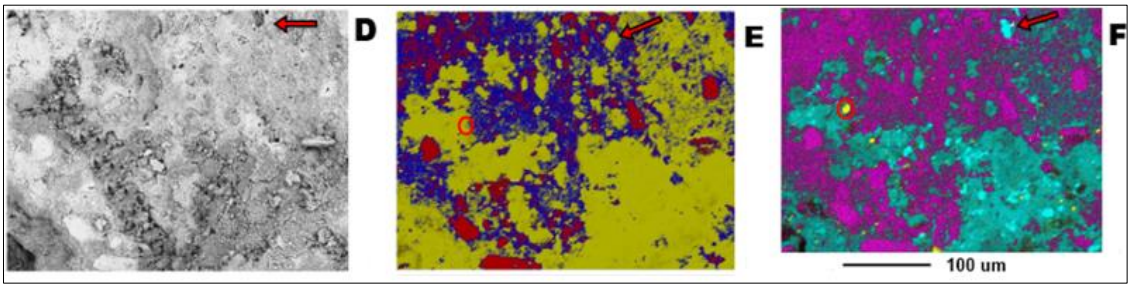

Fig. 10: EDS microanalysis by X-2D mapping of TSIAKI samples. Mineralogical composition of TSIAKI samples: mapping of mineral phases

From Figure 10, D) BSE (backscattered electrons) mode under low pressure conditions;

E) Mapping of statistical analysis of spectral data. The spectra representing the three phases are expressed in images 9 and 10 with a quantitative evaluation and mineralogical interpretation in atomic %. The yellow areas cover 65% of the surface and have a high kaolinite content. The red areas are richest in aluminum and iron oxides (goethite and gibbsite), while the blue areas are intermediate areas between the two previous stages. F) Overlays of Si, Fe and Ti mapping allow for a precise visualization of the regions with high contents of each atomic element. Areas highlighted in black were not identified by EDS. Using BSE (backscattered electrons), the details of the image obtained on the TSIAKI sample (Figure 10-D). The granular structure of this sample is different from that of TSANGA (Figure 9-A).

The entire surface of the image observed in Figure 10D was mapped in 2D using EDS X-ray microanalysis. The acquired 2D mappings are shown in Figure 10-E and F. As with the TSANGA sample, the X-ray microanalysis mapping data was analyzed by statistics. Figure 10-E shows the 3 phases obtained after mapping. The phases identified are associations of different amounts of iron oxide (aluminum) and kaolinite. The red areas (Fig.10-E) have a high concentration of iron oxides, 51% goethite associated with 14.7% gibbsite and 33.5% kaolinite. The blue areas have high kaolinite (43%) and low iron oxide (31% goethite and 8.9% gibbsite). The areas colored yellow (Fig.10-E) have high concentrations of kaolinite (62.5%) and a lower amount of iron oxides (16% goethite). Figures 11 and 12 show the mineralogical details of the three phases identified by EDS.

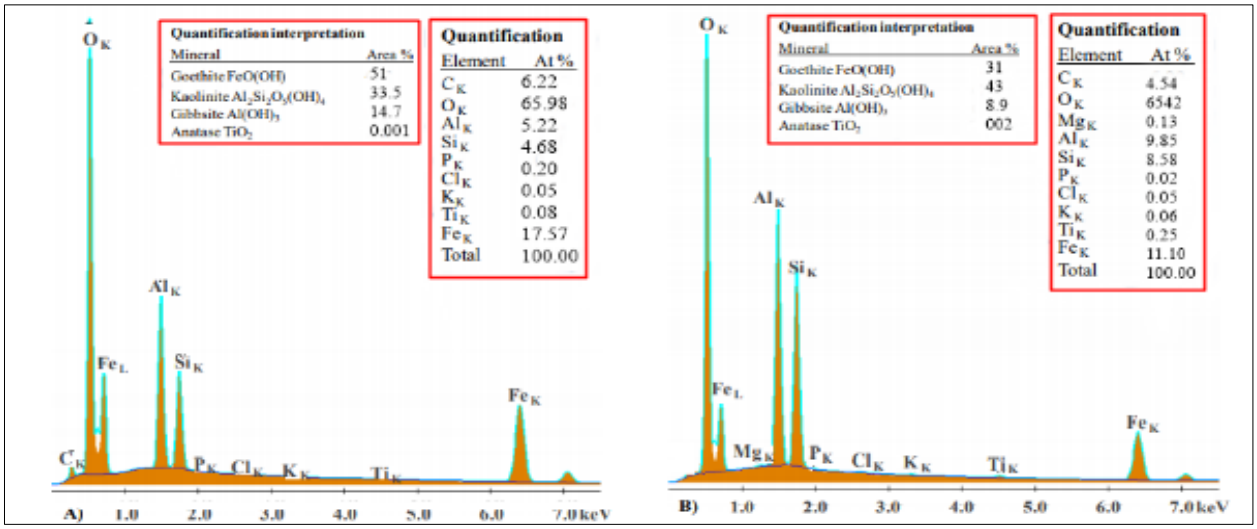

Fig. 11: Statistical analysis of the 2D mapping based on the phase reconstruction over the total area of the image in Figure 10-D

From Figure 11, A) Spectrum defining the red areas in Figure 10-E. Quantification in atomic percent (At %) indicates a mineral phase arrangement (% area occupied by the red phase) of 51% goethite, 33.5% kaolinite, 14.7% gibbsite and traces of anatase. B) Spectrum expressing the blue areas in Figure 10-E. The corresponding atomic percentage quantification shows a combination of kaolinite (43%), goethite (31%), gibbsite (8.9%) and trace anatase.

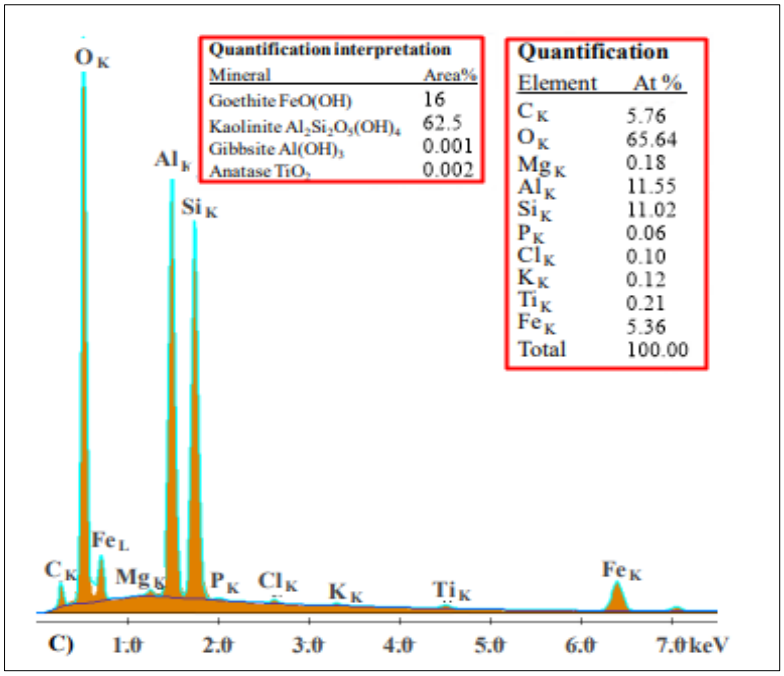

Fig. 12: Statistical analysis of the 2D mapping from the phase reconstruction over the entire surface of the image in Figure 10-D

Spectra showing the area highlighted in yellow in Figure 10-E. Quantification of the atomic percentage (At%) was described as the aggregation of the mineral phases (% of the total surface occupied by the phases shown in yellow in Figure 10-E, consisting of 62.5% kaolinite, 16% goethite). Some traces of gibbsite and anatase were identified.

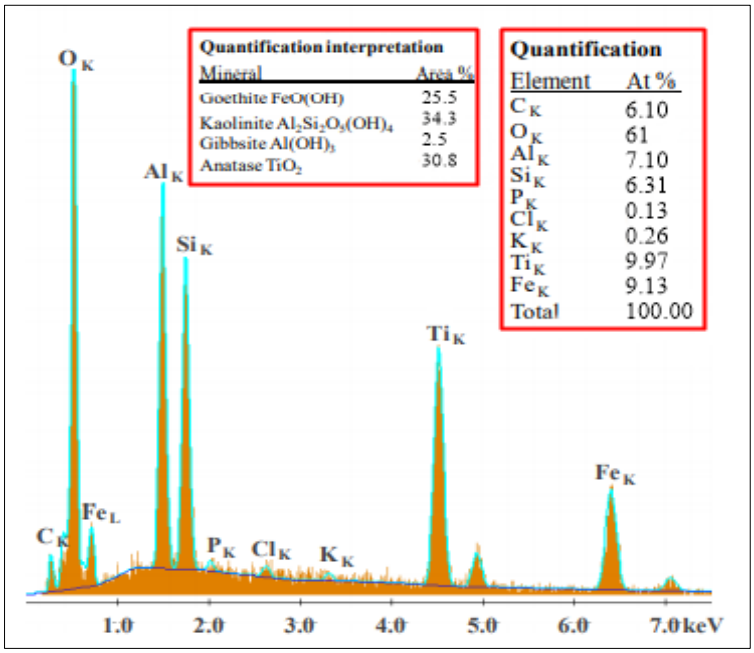

Fig. 13: Calculated spectrum over the region marked by the small red circle in Figure 10-F, characterizing titanium as yellow dots

The quantification in atomic % (Fig.13) reflects a mineral phase association consisting of 30.8% anatase, 25.5% goethite, 34.9% kaolinite and 2.5% gibbsite. As we have seen for T, the superposition of the elemental mappings (Ti, Fe and Si) in Figure 10-F demonstrates that each spectrum (Fig.11 and Fig.12) has been characterized with its corresponding phase (yellow, blue and red) in terms of its statistical mean. For example, Figure 13 shows the EDS spectrum measured over the Ti rich area representing the small circle in Figure 10-E and F that falls on the yellow phase (Fig.10-E). The EDS spectrum obtained at this location is interpreted as a composite (% occupancy) of 34.3% kaolinite, 30.8% anatase, 27.4% goethite and 2.5% gibbsite.

4. CONCLUSION

The tests carried out allowed the characterization of the geotechnical properties of two lateritic gravels which are of class B6. The results obtained show that the maximum dry density varies from DDM (1.95-2.198 t/m3), the optimum water content OMC (10.63-7.43%), the bearing indices CBR (27-68%) and the linear swelling Gf (0.4-0.7) respectively for the TSANGA and TSIAKI samples. The lateritic gravels of TSIAKI and TSANGA have respective fines contents of 23-30%. After compaction, the percentages of fines obtained are 27-35%, i.e., an increase in fines of 4% for the TSIAKI sample and 5% for the TSANGA sample. These increases of 4-5% are less than the maximum of 8%. This increase in fines depends on the frictional resistance of the material obtained by the Los Angeles 27-30 test. The TSANGA lateritic gravel has a plasticity index higher than 10%, the passing's at 0.425mm are higher than 15%, the fines content is lower than 35%, the maximum grain size is lower than 50 mm and its plasticity modulus is lower than 2500; conditions required for the material to be treated with hydraulic binders to improve its bearing capacity. However, TSIAKI's lateritic gravel has a CBR of 68% and can be significantly improved for use as a base course, if about 30% by weight of 0/40 angular stony aggregate is added, with less than 30% passing at 2mm and less than 18% passing at 80 µm, at a zero-plasticity index and CBR at 95% OPM of about 90. The methylene blue value of TSIAKI and TSANGA MBV (2.2-4.3 g/100g), between (2.5 <MBV< 6), i.e., the gravels have a medium plasticity. The mineralogical characterization allowed a precise qualitative and quantitative description of the different mineral phases identified in these soils.

These samples showed different textures compared to the mode of attack of the iron oxides. The TSANGA sample is represented by a texture with isolated ferruginous attacks whereas the attack of iron oxides is diffuse for the TSIAKI sample. The minerals common to these different textures are: quartz, kaolinite and iron oxides. The DRX analysis carried out on the samples apart from the three mineral phases found revealed two to three additional mineral phases mainly gibbsite, anatase and microcline. The quantification of the minerals obtained by XRD gives a precise idea of the content of each mineral. The TSANGA sample has a high quartz and kaolinite content and its CBR value is lower than that of TSIAKI.

Declarations

Conflict of Interest: The authors declare no competing interests.

RÉFÉRENCES

1. National Development Plan 2018-2022 of the Republic of Congo (2017).
2. United Nations Economic Commission for Africa. Transport situation in Africa (2007). Fifth session of the Committee on Trade and Cooperation and Regional Integration. Addis Abeba. E/ECA/CTRCI/5/3.
3. Louis, A. (2018). Improvement of the geotechnical properties of the lateritic gravel by adding crushed alluvial gravel 0/31.5. *Journal RAMReS 2018 – Applied and Engineering Sciences*, *3*(1), 1-6, Online January 2019. http://publication.lecames.org
4. Ekouya, A., Ahouet, L., & Okina, S. N. (2024). Collaborative Effect of Fines on Changes in Grain Distribution in the Process of Improving the Geotechnical Properties of an Alluvial Gravel 0/14. *Geomaterials*, *14*(3), 29-48.
5. Sangaré, M., & Atiase, S. (1991). Synthesis of data on rural road maintenance and rehabilitation in West and Central Africa. *African Development Support Project*, 698-0464.28
6. Cocks, G., Keeley, R., Leek, C., Foley, P., Bond, T., Cray, A., ... & Marchant, L. (2015). The use of naturally occurring materials for pavements in Western Australia. *Australian Geomechanics*, *50*(1), 43-106.
7. Okina, S. N. Louis Ahouet, Destin Gemeton Etou (2023). Evaluation of Concrete Performances Based Recycled Aggregates of Road and Build Demolition for a Formal Using in the Republic of Congo. *Saudi J Eng Technol*, *8*(11), 267-273.
8. Weinert, H. H (1980). *The natural road construction materials of South Africa*. Academica, Pretoria, Cape Town.
9. Molenaara, A. A. A. (2013). Durable and Sustainable Road Constructions for Developing Countries. *Procedia Engineering*, 54.
10. Riverson, J., Gaviria, J., Thriscutt, S. (2002). Rural Roads in Sub-Saharan Africa, Lessons from World Bank Experience. World Bank. Technical Paper, 141.
11. Nwaiwu, C. M. O., Alkali, I. B. K., & Ahmed, U. A. (2006). Properties of ironstone lateritic gravels in relation to gravel road pavement construction. *Geotechnical & Geological Engineering*, *24*, 283-298.
12. Far, S. Z., Kassim, K. A., Eisazadeh, A., & Khari, M. (2013). An evaluation of the tropical soils subjected physicochemical stabilization for remote rural roads. *Procedia engineering*, *54*, 817-826.

13. Elenga, R. G., Ahouet, L., Ngoulou, M., Bouyila, S., Dirras, G. F., & Kengué, E. (2019). Improvement of an alluvial gravel geotechnical properties with a clayey soil for the road construction. *Research Journal of Applied Sciences, Engineering and Technology*, *4*, 135-139.
14. Millogo, Y., Traoré, K., Ouedraogo, R., Kaboré, K., Blanchart, P., & Thomassin, J. H. (2008). Geotechnical, mechanical, chemical and mineralogical characterization of a lateritic gravels of Sapouy (Burkina Faso) used in road construction. *Construction and Building Materials*, *22*(2), 70-76.
15. Mahalinga-Iyer, U., & Williams, D. J. (1997). Properties and performance of lateritic soil in road pavements. *Engineering Geology*, *46*(2), 71-80.
16. Dadet, P. (1969). Explanatory note for the 1:500 000 geological map of the Republic of Congo: area between parallels 2° and 5° south. Editions BRGM.
17. AFNOR NF P94-056 (1996). Soil: investigation and testing – Granulometric analysis. Dry sieving method after washing, Marth 1996.
18. NF P94-057 (2018). The granulometric analysis by sieving of soil for grains smaller than 80µm, January 2018.
19. AFNOR NF P94-051 (1993). Soils: Reconnaissance and testing. Determination of Atterberg limits; Limit of liquidity at compelled – Limit of plasticity at Rouleau, Marth 1993.
20. AFNOR NF P 11 300 (1992). Construction of earthworks - Classification of materials for use in the construction of embankments and subgrades of road infrastructures - September 1992.
21. NF P94-068 (1998). Soils: Investigation and testing – Measuring of the methylene blue adsorption capacity of a rocky soil. Determination of the methylene blue of a soil by means of the strain test, October 1998.
22. AFNOR NF P94-093(1999). Soils: Reconnaissance and testing. Determination of the compaction references of a material, October 1999.
23. AFNOR NF P94-078 (1997). CBR index after immersion - Immediate CBR index - Immediate CBR bearing index, May 1997.
24. AFNOR NF EN 1097-2. Tests for determining the mechanical and physical properties of aggregates - Part 2: Methods for determining the resistance to fragmentation.
25. CEBTP (1980). Practical guide to pavement design for tropical countries. Ministry of Cooperation of the French Republic, 155 pages.
26. CEBTP (1984). Practical guide to pavement design for tropical countries. Ministry of External Relations - Cooperation and Development of the French Republic, 157 pages.
27. Zondjé Poanguy, B. B. (2008). Characterization of lateritic soils used in road construction: case of the Agneby region (Ivory Coast). Mechanics of materials. PhD thesis, National School of Bridges and road.
28. Souley Issiakou, M. (2016). Characterization and valorization of lateritic materials used in road construction in Niger. University of Bordeaux.
29. Ndiaye, M., Magnan, J. P., Cissé, I. K., & Cissé, L. (2013). Study of the improvement of laterites in Senegal by adding sand. *Bridge and road Laboratory Bulletin*, 280-281
30. Malomo, S. (1987). Mineralogy and chemistry of different fractions of some soil laterites from northeast Brazil. *Chem Geol*, *60*, 101–9.

